

SB-BEVFUSION: ENHANCING THE ROBUSTNESS AGAINST SENSOR MALFUNCTION AND CORRUPTIONS

Markus Essl¹, Marta Moscatti¹, Mubashir Noman², Muhammad Zaigham Zaheer²,
Usman Naseem³, Shah Nawaz¹, Markus Schedl^{1,4}

¹Johannes Kepler University Linz, Austria, ²MBZUAI, UAE,
³Macquarie University, Sydney, Australia, ⁴Linz Institute of Technology, Austria

ABSTRACT

Multimodal sensor fusion has demonstrated remarkable performance improvements over unimodal approaches in 3D object detection for autonomous vehicles. Typically, existing methods transform multimodal data from independent sensors, such as camera and LiDAR, into a unified bird’s-eye view (BEV) representation for fusion. Although effective in ideal conditions, this strategy suffers from substantial performance deterioration when camera or LiDAR data are missing, corrupted, or noisy. To address this vulnerability, we develop a framework-agnostic fusion module for camera and LiDAR data that allows for handling cases when one of the two modalities is missing or corrupted. To demonstrate the effectiveness of our module, we instantiate it in BEVFusion [1], a well-established framework to combine camera and LiDAR data for 3D object detection. By means of quantitative experiments on the MultiCorrupt dataset, we demonstrate that our module achieves favorable performance improvements under scenarios of missing and corrupted modalities, substantially outperforming existing unified representation approaches across a wide range of sensor deterioration scenarios and reaching state-of-the-art performance in scenarios of corrupted modality due to extreme weather conditions and sensor failure.

Index Terms— Sensor fusion, 3D object detection, Modality corruption

1. INTRODUCTION

Perception in self-driving cars is predominantly dependent on two complementary sensors: *camera* and *LiDAR* [2]. The former sensor is responsible for rich visual appearance, while the latter offers the precise geometry necessary for accurate detection of objects [3]. To exploit this complementary information from camera and LiDAR, techniques for Bird’s-Eye View (BEV) such as BEVFusion [4, 1] propose to fuse these two modalities, assuming that both are present and of high quality. However, real-world scenarios are not ideal and may lead to corrupted data, resulting in substantial performance deterioration of such systems [5, 6, 7]. These scenarios in-

clude situations like adverse weather conditions affecting the visibility from the camera, such as fog, rain, and malfunctions affecting the LiDAR system, such as beam reduction and occlusion [8, 9, 10]. Furthermore, spatial and temporal misalignment between the two modalities may cause considerable deterioration of the systems. Addressing these situations is an emerging field of research. For example, a recent work [10] has mainly focused on curating a benchmark to evaluate the state-of-the-art (SOTA) multimodal 3D detectors on their robustness against sensor failures or corruptions.

To this end, we set out to develop a fusion technique capable of robustly handling corrupted or missing modalities, and at the same time, it can be seamlessly integrated as a fusion module in existing architectures. Specifically, we introduce a single-branch BEV detector (SB-BEV Fusion) that allows the model to maintain good performance when camera or LiDAR data is missing. When both modalities are clean and present, the BEV features are combined by means of a pipeline relying on unweighted averaging, max pooling, cross-attention, and progressive modality decay. When one modality is absent or corrupted, our proposed architecture passes the available BEV representations without fusion. The novelty of our model relies on the fact that the downstream network and the detection head are shared across both modalities (camera (C) and LiDAR (L)) and trained on a shuffled mixture of L+C/L/C. This allows our model to handle both unimodal and multimodal scenarios in an effective way, therefore tackling the case of missing modality effectively. In summary, our main contributions are as follows.

- We investigate various fusion strategies to combine the multimodal BEV feature representations, focusing on their robustness to missing and corrupted modality.
- We introduce a module that is designed to explicitly operate under L+C/L/C scenarios.
- We conduct extensive experiments on the MultiCorrupt dataset and empirically demonstrate that our proposed module demonstrates improved robustness towards the scenarios of missing and corrupted modality.

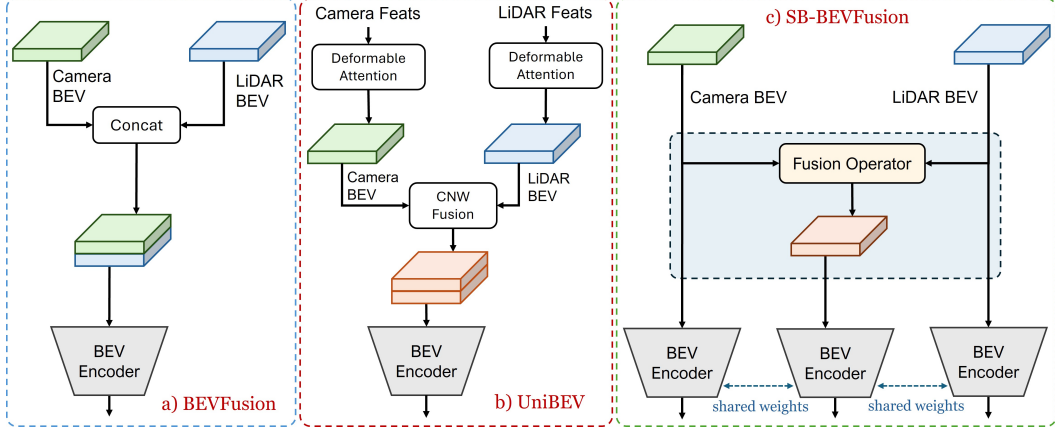


Fig. 1. Comparison between proposed **SB-BEV Fusion**, BEVFusion [1], and UniBEV [11]. a) Camera and LiDAR data is processed by modality-specific encoders to obtain features which are transformed to camera and LiDAR BEV representations. Afterwards, these BEV features are concatenated and processed by BEV encoder. b) UniBEV uses deformable attention before transformation to BEV space. It utilizes Channel Normalized Weights (CNW) fusion module to combine the BEV representations and feed them to BEV encoder. c) Proposed SB-BEV Fusion does not add complexity to the architecture and combines the BEV representations using a fusion operator \mathcal{F} when both modalities are available or acts as an identity when one of them is absent. A shared BEV encoder processes the BEV features \mathbf{F}_{in} in all modes to obtain 3D detections.

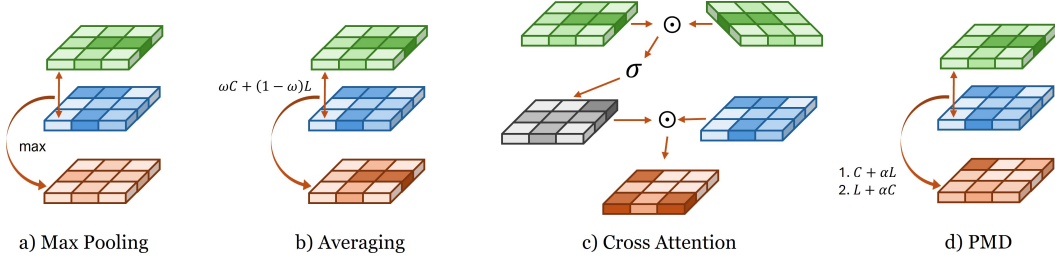


Fig. 2. Illustration of various fusion operations to combine the BEV feature representations utilized in this study.

2. METHODOLOGY

Setup and Notation. We adopt the pipeline of BEVFusion [1], depicted in Fig. 1, as underlying framework to apply our fusion module. As in BEVFusion, we first extract feature representations utilizing modality-specific encoders for the LiDAR point cloud \mathbf{P} and for the multi-view camera images $\mathbf{I} = \{I_k\}_{k=1}^K$, where K represents the number of camera views. These representations are then projected to a unified BEV space preserving the semantic and geometric information. The resulting representations in BEV space are given by

$$\tilde{\mathbf{F}}_{\text{cam}} \in \mathbb{R}^{H \times W \times C_{\text{cam}}}, \quad \tilde{\mathbf{F}}_{\text{lid}} \in \mathbb{R}^{H \times W \times C_{\text{lid}}} \quad (1)$$

where H, W, C represent the height, width, and number of channels, respectively. BEVFusion combines $\tilde{\mathbf{F}}_{\text{cam}}$ and $\tilde{\mathbf{F}}_{\text{lid}}$, with simple concatenation \mathcal{F} , obtaining the multimodal representation which is fed to a convolutional BEV encoder \mathcal{E} , designed to adjust the local misalignments that can occur due to inaccurate depth.

$$\mathbf{F}_{\text{fused}} = \mathcal{F}(\tilde{\mathbf{F}}_{\text{lid}}, \tilde{\mathbf{F}}_{\text{cam}}), \quad \hat{\mathbf{y}} = \mathcal{E}(\mathbf{F}_{\text{fused}}) \quad (2)$$

It is well-known that the fusion operation is critical for effective combination of multimodal information [12, 13]. This motivated us to investigate various fusion schemes and analyze their impact on improving model performance under different sensor corruptions. Moreover, our concern for the model robustness against sensor failure further encouraged us to introduce the SB-BEV Fusion, which is based on effective training strategy and fusion operators and does not assume both modalities to be present.

To this end, we first equalize channel widths such that $C_{\text{cam}} = C_{\text{lid}} \triangleq C$, yielding BEV tensors of same dimensions. This allows us to apply fusion \mathcal{F} when both modalities are present and only pass the features of the available modality to the BEV encoder otherwise, as illustrated in Fig. 1.

$$\mathbf{F}_{\text{in}} = \begin{cases} \mathcal{F}(\tilde{\mathbf{F}}_{\text{lid}}, \tilde{\mathbf{F}}_{\text{cam}}), & a_{\text{lid}} \wedge a_{\text{cam}}, \\ \tilde{\mathbf{F}}_{\text{lid}}, & a_{\text{lid}}, \\ \tilde{\mathbf{F}}_{\text{cam}}, & a_{\text{cam}}. \end{cases} \quad \hat{\mathbf{y}} = \mathcal{E}(\mathbf{F}_{\text{in}}) \quad (3)$$

Fusion Operators. The fusion operator \mathcal{F} is responsi-

ble for mapping the same-sized multimodal BEV representations into a combined single BEV tensor, given by $\mathbf{F}_{\text{in}} = \mathcal{F}(\tilde{\mathbf{F}}_{\text{lid}}, \tilde{\mathbf{F}}_{\text{cam}}) \in \mathbb{R}^{H \times W \times C}$. The fusion operator is applied when both modalities are present and is replaced by the identity function when one modality is missing. The fusion operators investigated in our approach are depicted in Fig. 2.

1. **Averaging:** We first combine the camera and LiDAR BEV representations by using unweighted average fusion. This is given by:

$$\mathbf{F}_{\text{in}} = w \tilde{\mathbf{F}}_{\text{cam}} + (1 - w) \tilde{\mathbf{F}}_{\text{lid}}, \quad w = 0.5 \quad (4)$$

2. **Max-Pooling:** We apply the max-pooling operation on the two BEV representations and retain features given by:

$$\mathbf{F}_{\text{in}} = \max(\tilde{\mathbf{F}}_{\text{lid}}, \tilde{\mathbf{F}}_{\text{cam}}) \quad (\text{element-wise over } H \times W \times C) \quad (5)$$

3. **Cross-Attention:** Motivated by the performance improvement on other multimodal domains [14, 15], we utilize cross-attention to merge the camera and LiDAR BEV features to obtain the refined fused representations. Mathematically, this operation is given by:

$$\mathbf{F}_{\text{in}} = \tilde{\mathbf{F}}_{\text{lid}} + \gamma W_o \text{Attn}(W_q \tilde{\mathbf{F}}_{\text{lid}}, W_k \tilde{\mathbf{F}}_{\text{cam}}, W_v \tilde{\mathbf{F}}_{\text{cam}}) \quad (6)$$

Here, $\text{Attn}(\cdot)$ is standard multi-head attention; $W_{\{\cdot\}}$ are 1×1 projections; we flatten $C \times H \times W$ to HW tokens inside Attn and reshape back afterwards; $\gamma = \sigma(\theta)$ is a scalar gate.

4. **Progressive Modality Decay (PMD):** To encourage the model to adapt to the missing-modality case, we combine the BEV representations in a modality-decay fashion. In this case, one modality is kept constant while second modality is multiplied by a decaying factor α and added to the first modality. For each training example, an anchor modality is chosen. The fused BEV features are obtained as:

$$\mathbf{F}_{\text{in}} = \tilde{\mathbf{F}}_{\text{anchor}} + \alpha \tilde{\mathbf{F}}_{\text{other}} \quad (7)$$

where α decays from 1 (start of training) to 0 (end).

Among the investigated fusion operators, *Averaging* demonstrates superior performance, as detailed in Table 1. Therefore, this is a default choice in our experiments, unless specifically stated otherwise.

Training Schedules. Following prior work [16, 17, 18, 19, 20], we train a single downstream path to operate under three regimes: L+C, L, and C. For the average, max-pooling and cross-attention fusion strategies, we enumerate all three regimes per sample; for PMD, we enumerate two anchored passes (LiDAR-anchored and camera-anchored). The expanded epoch is globally shuffled so each mini-batch mixes regimes. Concrete epoch counts are given in Sec. 3.

Inference. During inference time, we utilize the fusion operator only when both modalities are available. If one modality is missing, the fusion operator becomes the identity, and the model runs with only one modality as input, with no other structural change. This scheme enables the model to handle missing-modality scenarios and enhance its robustness.

3. EXPERIMENTS

Dataset. We evaluated our proposed strategies on the nuScenes dataset [21]. This is a large-scale multimodal benchmark dataset for autonomous driving, providing full 360° coverage, including six cameras, one 32-beam LiDAR, and five radars; this study focuses on LiDAR and camera data streams, and we therefore discard the radar data. The dataset comprises 1,000 scenes, each 20 seconds long. These scenes were captured in Boston (USA) and Singapore, and provide samples of varied driving conditions, times of day (day/night), and weather conditions (e.g., clear, rain). The dataset also provides rich 3D bounding box annotations for 23 object classes; the 10 common classes from the official nuScenes detection challenge are used for 3D object detection. Model training and evaluation use the official nuScenes train and val splits with 850 and 150 scenes, respectively, for consistency with established benchmarks. We applied standard pre-processing steps, aligned with common BEVFusion methodologies [1]. Camera images are resized to a fixed resolution and normalized. For LiDAR data, points from the previous 10 sweeps are accumulated to form a denser point cloud for the current frame. These accumulated points are transformed into the current ego-vehicle’s reference frame, accounting for vehicle motion and sensor extrinsic calibration. Moreover, we use the MultiCorrupt [10] dataset as a benchmark to evaluate our method against various corruption categories and severity levels. The dataset was intentionally corrupted to simulate challenging real-world environmental conditions. Corruption severity is defined across three levels, following the MultiCorrupt benchmark: Level 1 introduces minor perturbations to simulate mild environmental noise, Level 2 applies medium-strength distortions, and Level 3 imposes severe corruption to replicate extreme failure scenarios.

Metrics and Protocol. We report the standard nuScenes detection metrics: mean Average Precision (mAP) and nuScenes Detection Score (NDS). Unless stated otherwise, all results are on the official val split. We evaluate three modality-availability regimes: **L+C** (both sensors), **L** (LiDAR only), and **C** (camera only). Moreover, we evaluate robustness with MultiCorrupt [10] on nuScenes val, using 5 corruption families including LiDAR beam reduction, spatial misalignment, temporal misalignment, fog, and motion blur. Unless stated otherwise, corruptions are applied to raw sensor streams prior to BEV projection, with three severities $s1$ – $s3$. Besides the standard NDS, we report the *mean Resistance Ability (mRA)*, defined as the average over corruption families and severities of the ratio between a metric \mathcal{M}

Table 1. Comprehensive NDS comparison of SB-BEVFusion variants, fusion strategies, and SOTA under corruptions. Abbreviations: BEVF (BEVFusion), UniBEV (UniBEV_cnw), BEVFusion-D (Decay), BEVFusion-Avg (Avg), BEVFusion-CA (Cross-Attention), BEVFusion-MP (Max-Pool).

Corruption	Sev.	BEVF	UniBEV	SB-BEVFusion-D	SB-BEVFusion-Avg	SB-BEVFusion-CA	SB-BEVFusion-MP
Beam Reducing	s1	0.6338	0.6181	0.5764	0.6219	0.6380	0.6365
	s2	0.4818	0.5061	0.4213	0.4821	0.4840	0.4954
	s3	0.3052	0.3981	0.2774	0.3192	0.3181	0.3303
Camera Fog	s1	0.6476	0.6363	0.6064	0.6464	0.6542	0.6520
	s2	0.5978	0.5931	0.5600	0.5999	0.6072	0.6043
	s3	0.3453	0.3648	0.3466	0.3565	0.3740	0.3615
Motion Blur	s1	0.6687	0.6348	0.6287	0.6629	0.6789	0.6769
	s2	0.5865	0.5344	0.5447	0.5912	0.6060	0.6033
	s3	0.4991	0.4427	0.4634	0.5199	0.5250	0.5246
Spatial Misalignment	s1	0.5836	0.5794	0.5293	0.5917	0.5820	0.5896
	s2	0.4937	0.5065	0.4368	0.5110	0.4891	0.5032
	s3	0.4243	0.4492	0.3682	0.4408	0.4215	0.4351
Temporal Misalignment	s1	0.6276	0.6122	0.5920	0.6254	0.6348	0.6351
	s2	0.5394	0.5292	0.5091	0.5405	0.5480	0.5480
	s3	0.4676	0.4646	0.4456	0.4705	0.4785	0.4768
Mean Resistance Ability		0.7490	<u>0.7656</u>	0.7313	0.7683	0.7537	0.7592

Table 2. Overall performance on nuScenes validation set with multiple missing sensor configurations. Best results are bold; second best are underlined.

Modality Availability	mAP \uparrow			NDS \uparrow		
	SB-BEVFusion (Avg)	BEVFusion	UniBEV	SB-BEVFusion (Avg)	BEVFusion	UniBEV
Both Modalities	0.6737	<u>0.6691</u>	0.642	<u>0.6970</u>	0.7033	0.685
Camera Only	<u>0.2002</u>	0.0109	0.35	0.2440	0.1074	0.424
LiDAR Only	0.6448	0.5639	<u>0.582</u>	0.6959	0.5361	<u>0.653</u>

measured under corruption and its value on clean data; in our experiments, $\mathcal{M} = \text{NDS}$:

$$\text{mRA} = \frac{1}{3N} \sum_{c=1}^N \sum_{s=1}^3 \frac{\mathcal{M}_{c,s}}{\mathcal{M}_{\text{clean}}}.$$

Implementation Details. We match the official BEVFusion configuration and initialize from a parity checkpoint. The only deviations from the public config are: (i) we set the camera BEV projection width to match the LiDAR BEV channels so that $C_{\text{cam}} = C_{\text{lid}} (\hat{=} C)$, we also apply this change when training the BEVFusion baseline, and use that checkpoint for all ablations; (ii) for SB-BEVFusion we replace the two-branch concat+conv with our single-branch module defined in Sec. 2 while preserving the BEV tensor interface; and (iii) we train with availability mixing by enumerating $\{\text{L+C}, \text{L}, \text{C}\}$ per sample and shuffling the expanded epoch. Upstream encoders are frozen to isolate downstream effects. We train the 3-regime operators for 3 epochs and PMD for 4 epochs over their expanded datasets.

4. RESULTS AND DISCUSSION

Robustness Against Corrupted Sensor Modalities. Table 1 provides an extensive performance evaluation of our method alongside other SOTA strategies under various types

of corruptions. The experimental results demonstrate that all methods experience performance deterioration as the severity of corruptions increases, but the extent of degradation varies across approaches. For beam reduction and motion blur, the attention-based fusion methods (e.g., SB-BEVFusion-CA and SB-BEVFusion-MP) maintain relatively stronger robustness compared to other variants. Under camera fog, most methods achieve competitive results, with SB-BEVFusion-CA slightly outperforming others. For spatial and temporal misalignments, SB-BEVFusion-CA consistently shows superior resilience across different severities. When averaged across all corruptions, SB-BEVFusion-Avg achieves the highest mean resistance ability (0.7683), closely followed by UniBEV (0.7656), SB-BEVFusion-MP (0.7592). These findings highlight that different fusion strategies have varying sensitivity to corruption types, with attention- and averaging-based fusion methods showing the most stable performance.

Robustness Against Missing Sensor Modalities. Although corruption affects the overall quality of a sensor, some information may still be retained, which the network may use to perform the detection task. In this section, we consider a more extreme scenario, i.e., the setting in which a sensor is completely removed. This may be considered a corner case where no data regarding the corrupted sensor is avail-

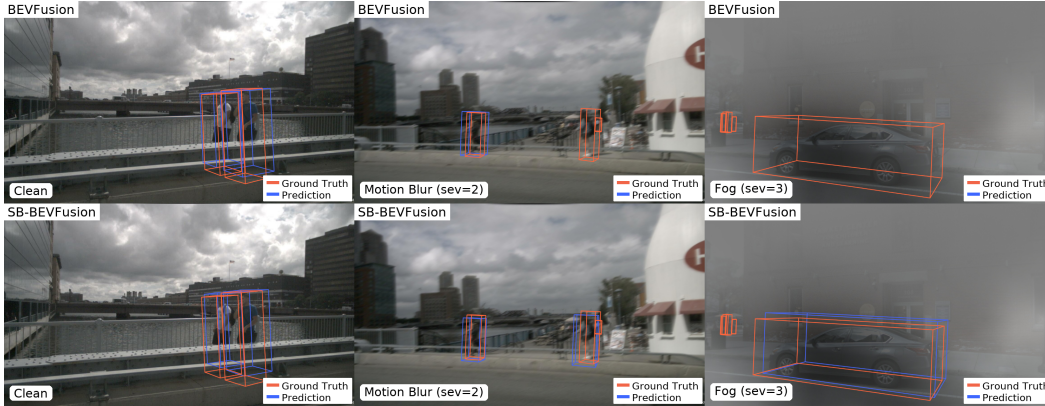


Fig. 3. Qualitative comparison of BEVFusion (top) vs. SB-BEVFusion (bottom). Panels show Clean, Motion Blur (severity 2), and Fog (severity 3). Under corruptions, SB-BEVFusion remains robust compared to BEVFusion’s predictions, matching quantitative trends. We observe that BEVFusion detection performance deteriorates notably with increasing severity level, i.e. Motion Blur and Fog.

able to the network. Table 2 presents a comprehensive evaluation of our method alongside other SOTA strategies under various conditions of missing sensor data. The results demonstrate a clear trade-off between peak performance and robustness across the evaluated models. When both camera and LiDAR data are available, our method, SB-BEVFusion, achieves the highest detection precision (mAP of 0.6737). Under sensor failure scenarios, a notable performance contrast emerges: UniBEV proves substantially more robust in camera-only settings (mAP 0.35), outperforming other approaches. We conjecture that such favorable performance is obtained due to the utilization of deformable attention before transforming the multiview camera features into BEV representations. Conversely, in the LiDAR-only condition, our method excels (mAP 0.6448), demonstrating superior robustness. These findings indicate that while BEVFusion performs well under ideal sensing conditions, our approach maintains competitive performance in full sensor settings while exhibiting superior LiDAR-only robustness. In contrast, UniBEV shows distinctive resilience to camera-only operation.

Qualitative Analysis. Fig. 3 presents a qualitative comparison between BEVFusion (top row of each panel) and our SB-BEVFusion (bottom row of each panel) under different corruption scenarios. On clean data, both methods provide accurate predictions closely aligned with the ground truth. However, under corruptions such as motion blur (severity level 2) and fog (severity level 3), differences in performance become evident. We observe from Fig. 3, even notably large objects are not detected by BEVFusion when fog severity level is highest. In general, BEVFusion exhibits deteriorated detection performance, with predicted bounding boxes deviating more noticeably from the ground truth. Alternatively, SB-BEVFusion produces more accurate predictions under the same conditions, maintaining better alignment with the ground truth boxes despite the presence of corruptions. These

qualitative results confirm the quantitative findings, highlighting that SB-BEVFusion is more resilient to corruptions, especially under severe conditions.

5. CONCLUSION

In this work, we proposed SB-BEVFusion method that improves the robustness of the model against sensor corruption and failure. The paper investigated several fusion operators to effectively combine multimodal BEV representations and demonstrated that unweighted averaging provides superior overall performance compared to other fusion operators. Extensive experimentation on MultiCorrupt dataset demonstrated that the concatenation operation for BEV feature fusion is suboptimal and requires careful considerations for selecting the effective fusion operations depending on the corruption type. In addition, utilizing the shuffled mixture of L+C/L/C scenarios for model training improves its robustness against modality failure. One of the limitations of the proposed work is that, although SB-BEVFusion would allow fusing other modalities (e.g., radar) after converting them to BEV, we only tested it on camera and LiDAR data. Our potential future direction is to further investigate and improve performance of transformer based fusion methods.

6. ACKNOWLEDGMENTS

This research was funded in whole or in part by the Austrian Science Fund (FWF): Cluster of Excellence *Bilateral Artificial Intelligence* (<https://doi.org/10.55776/COE12>), the doc.funds.connect project *Human-Centered Artificial Intelligence* (<https://doi.org/10.55776/DFH23>), and the PI project *Intent-aware Music Recommender Systems* (<https://doi.org/10.55776/P36413>). For open access purposes, the authors have applied a CC BY public copyright license to any author-accepted manuscript version arising from this submission.

7. REFERENCES

- [1] Zhijian Liu, Haotian Tang, Alexander Amini, Xingyu Yang, Huihui Mao, Daniela Rus, and Song Han, “Bevfusion: Multi-task multi-sensor fusion with unified bird’s-eye view representation,” in *IEEE International Conference on Robotics and Automation (ICRA)*, 2023.
- [2] Junjie Yan, Yingfei Liu, Jianjian Sun, Fan Jia, Shuailin Li, Tiancai Wang, and Xiangyu Zhang, “Cross modal transformer: Towards fast and robust 3d object detection,” in *Proceedings of the IEEE/CVF international conference on computer vision*, 2023, pp. 18268–18278.
- [3] Di Feng, Christian Haase-Schütz, Lars Rosenbaum, Heinz Hertlein, Claudius Glaeser, Fabian Timm, Werner Wiesbeck, and Klaus Dietmayer, “Deep multi-modal object detection and semantic segmentation for autonomous driving: Datasets, methods, and challenges,” *IEEE Transactions on Intelligent Transportation Systems*, vol. 22, no. 3, pp. 1341–1360, 2020.
- [4] Tingting Liang, Hongwei Xie, Kaicheng Yu, Zhongyu Xia, Zhiwei Lin, Yongtao Wang, Tao Tang, Bing Wang, and Zhi Tang, “Bevfusion: A simple and robust lidar-camera fusion framework,” *Advances in Neural Information Processing Systems*, vol. 35, pp. 10421–10434, 2022.
- [5] Muhammad Irzam Liaqat, Qaiser Abbas, Shah Nawaz, Zaigham Zaheer, Marta Moscati, Yufang Hou, Muhammad Haris Khan, Salman Khan, Elisabeth Andre, and Markus Schedl, “Multimodal learning under imperfect data conditions: A survey,” *Authorea Preprints*, 2025.
- [6] Kaicheng Yu, Tang Tao, Hongwei Xie, Zhiwei Lin, Tingting Liang, Bing Wang, Peng Chen, Dayang Hao, Yongtao Wang, and Xiaodan Liang, “Benchmarking the robustness of lidar-camera fusion for 3d object detection,” in *Proceedings of the IEEE/CVF Conference on Computer Vision and Pattern Recognition*, 2023, pp. 3188–3198.
- [7] Konyul Park, Yecheol Kim, Daehun Kim, and Jun Won Choi, “Resilient Sensor Fusion under Adverse Sensor Failures via Multi-Modal Expert Fusion,” 2025.
- [8] Shaoyuan Xie, Lingdong Kong, Wenwei Zhang, Jiawei Ren, Liang Pan, Kai Chen, and Ziwei Liu, “Benchmarking bird’s eye view detection robustness to real-world corruptions,” in *International Conference on Learning Representations 2023 Workshop on Scene Representations for Autonomous Driving*, 2023.
- [9] Yinpeng Dong, Caixin Kang, Jinlai Zhang, Zijian Zhu, Yikai Wang, Xiao Yang, Hang Su, Xingxing Wei, and Jun Zhu, “Benchmarking robustness of 3d object detection to common corruptions,” in *Proceedings of the IEEE/CVF Conference on Computer Vision and Pattern Recognition*, 2023, pp. 1022–1032.
- [10] Till Beemelmans, Quan Zhang, Christian Geller, and Lutz Eckstein, “Multicorrupt: A multi-modal robustness dataset and benchmark of lidar-camera fusion for 3d object detection,” in *2024 IEEE Intelligent Vehicles Symposium (IV)*. IEEE, 2024, pp. 3255–3261.
- [11] Shiming Wang, Holger Caesar, Liangliang Nan, and Julian FP Kooij, “Unibev: Multi-modal 3d object detection with uniform bev encoders for robustness against missing sensor modalities,” in *2024 IEEE Intelligent Vehicles Symposium (IV)*, 2024, pp. 2776–2783.
- [12] John Edison Arevalo Ovalle, Tamar Solorio, Manuel Montesy-Gómez, and Fabio A. González, “Gated multimodal units for information fusion,” in *5th International Conference on Learning Representations, ICLR 2017, Toulon, France, April 24-26, 2017, Workshop Track Proceedings*. 2017, OpenReview.net.
- [13] Muhammad Saad Saeed, Muhammad Haris Khan, Shah Nawaz, Muhammad Haroon Yousaf, and Alessio Del Bue, “Fusion and orthogonal projection for improved face-voice association,” in *ICASSP 2022-2022 IEEE International Conference on Acoustics, Speech and Signal Processing (ICASSP)*. IEEE, 2022, pp. 7057–7061.
- [14] Tao Liang, Guosheng Lin, Lei Feng, Yan Zhang, and Fengmao Lv, “Attention is not enough: Mitigating the distribution discrepancy in asynchronous multimodal sequence fusion,” in *Proceedings of the IEEE/CVF International Conference on Computer Vision*, 2021, pp. 8148–8156.
- [15] Jifeng Shen, Yifei Chen, Yue Liu, Xin Zuo, Heng Fan, and Wankou Yang, “Icafusion: Iterative cross-attention guided feature fusion for multispectral object detection,” *Pattern Recognition*, vol. 145, pp. 109913, 2024.
- [16] Michael Tschannen, Basil Mustafa, and Neil Houlsby, “Clippo: Image-and-language understanding from pixels only,” in *Proceedings of the IEEE/CVF conference on computer vision and pattern recognition*, 2023, pp. 11006–11017.
- [17] Muhammad Irzam Liaqat, Shah Nawaz, Muhammad Zaigham Zaheer, Muhammad Saad Saeed, Hassan Sajjad, Tom De Schepper, Karthik Nandakumar, Muhammad Haris Khan, Ignazio Gallo, and Markus Schedl, “Chameleon: A multimodal learning framework robust to missing modalities,” *International Journal of Multimedia Information Retrieval*, vol. 14, no. 2, pp. 21, 2025.
- [18] Christian Ganhör, Marta Moscati, Anna Hausberger, Shah Nawaz, and Markus Schedl, “Single-branch network architectures to close the modality gap in multimodal recommendation,” *ACM Transactions on Recommender Systems*, 2025.
- [19] Christian Ganhör, Marta Moscati, Anna Hausberger, Shah Nawaz, and Markus Schedl, “A multimodal single-branch embedding network for recommendation in cold-start and missing modality scenarios,” in *Proceedings of the 18th ACM conference on recommender systems*, 2024, pp. 380–390.
- [20] Muhammad Saad Saeed, Shah Nawaz, Muhammad Zaigham Zaheer, Muhammad Haris Khan, Karthik Nandakumar, Muhammad Haroon Yousaf, Hassan Sajjad, Tom De Schepper, and Markus Schedl, “Modality invariant multimodal learning to handle missing modalities: A single-branch approach,” *arXiv preprint arXiv:2408.07445*, 2024.
- [21] Holger Caesar, Varun Bankiti, Alex H Lang, Sourabh Vora, Venice Erin Liong, Qiang Xu, Anush Krishnan, Yu Pan, Giancarlo Baldan, and Oscar Beijbom, “nuscenes: A multimodal dataset for autonomous driving,” in *Proceedings of the IEEE/CVF conference on computer vision and pattern recognition*, 2020, pp. 11621–11631.